Wu, C., Nittrouer, J.A., Barefoot, E.A., and Burmeister, K.C., 2022, Reconstructing backwater hydrodynamics from fluvial-deltaic deposits using stratigraphic inversion: An example from the Tullig Sandstone, Western Irish Namurian Basin, County Clare, Ireland: GSA Bulletin, https://doi.org/10.1130/B36475.1.

Supplemental Material

Supplemental Text.

Figure S1. Geologic cross sections of characteristic first-order fault related folds deforming strata within the WINB.

Table S1. Outcrop locations.

Figure S2. Channel bed slope S versus friction coefficient C_f of 231 rivers (Li et al., 2015) with a power regression fit (A).

Figure S3. Inversion analyses for testing the sensitivity of model output to friction coefficient C_f (A–C) and bankfull normal flow depth H_n (D–F).

Supplemental Data.

Supplemental Material

Reconstructing backwater hydrodynamics from fluvial-deltaic deposits using stratigraphic inversion: an example from the Tullig Sandstone, Western Irish Namurian Basin, Co. Clare, Ireland

Chenliang Wu[1], Jeffrey A. Nittrouer[2], Eric A. Barefoot[3], Kurtis C. Burmeister[4]

[1]Department of Earth System Sciences, Yonsei University, Seoul, Republic of Korea, 03722

[2]Department of Geosciences, Texas Tech University, Lubbock, TX, 79409

[3]Department of Earth and Atmospheric Sciences, Indiana University, Bloomington, IN, 47408

[4]Geology Department, California State University, Sacramento, CA, 95819

Tectonic History of the Western Irish Namurian Basin

The pre-depositional tectonic history of the Western Irish Namurian Basin (WINB) is characterized by a series of Paleozoic lithospheric plate interactions that culminated in the Caledonian-Appalachian orogeny and formed the basement of the northwestern margin of Europe (Windley, 1995). During the Cambrian, the Avalonian microcontinent rifted from Gondwana, leading to the formation of the Rheic Ocean and the beginning of the closure of the Iapetus Ocean. Avalonia collided first with Baltica and then Laurentia during the Silurian and Devonian, forming the Iapetus suture (Windley, 1995; Murphy et al., 2001). Subsequent collisions with the Armorican microcontinent and Gondwana during the Permian trapped Avalonia within the center of Pangea (Neuman, 1984). Early Mesozoic rifting of the Pangean supercontinent ultimately led to the formation of the Atlantic Ocean, distributing fragments of the Avalonian microcontinent across North America, Spain, central Europe, the United Kingdom, and Ireland.

The post-depositional tectonic evolution of the WINB is dominated by deformation associated with the Variscan orogeny. The hinterland of the Variscan orogeny in southern Ireland is located approximately 40 km south of the Loop Head peninsula. Development of the foreland fold-thrust belt associated with the Variscan orogeny involved the upper Paleozoic sedimentary succession in the WINB in a series of East-West trending, kilometer-scale thrust-related folds (Fig. 3F; Cooper et al., 1986). Deformation in the fold-thrust belt decreases in both intensity and scale northwards towards a pin line near the latitude of the Cliffs of Moher (Figs. 1 and 3F; Gill, 1962; Naylor, 1978; Cooper et al., 1986; Tanner et al., 2011).

Structural Restoration

Since this study integrates field measurements with numerical modeling of sediment dispersal and accumulation, it is crucial to establish a robust spatial control on bedrock exposures in the Western Irish Namurian Basin (WINB). The first step in developing this framework is the geologic mapping and the systematic measurement of strata involved in structures within the WINB to characterize accurately pre-Variscan geometries and orientations. The results of this analysis provide the spatial control necessary to reconstruct pre-deformation distances – both vertically and horizontally – between the key bedrock exposures of the Tullig Sandstone. Strike-and-dip measurements (n = 203) of key stratigraphic surfaces in the WINB fluvial-deltaic sections from Tullig Point to Furreera were collected to resolve the location, geometry, and scale of first-order Variscan fault-related folds in the study area (Fig. 3F-G). Two previously inferred thrust faults (Tanner et al., 2011) were located and measured at Quilty (Figs. 1 and 3). Key stratigraphic surfaces bounding the depositional units (e.g., near-shore marine, channel mouth bar, and fluvial) and the initial and maximum flooding surfaces, marked by marine goniatite bands, were also identified in the field (Fig. 3F-G). The results of these field analyses were used to compile six geologic cross sections oriented perpendicular to the regional structural trends (northeast; Fig. s1). Preliminary line-length restorations of these cross sections suggest these first order structures accommodated 5-7% total horizontal shortening of the stratigraphic succession in a NW-SE direction. A parallel analysis of

grain-scale rock fabrics conducted by Lopez et al. (2017) on samples collected from the Ross Formation indicate that the contribution of penetrative strain to regional, layer-parallel shortening of strata within the WINB is negligible. These analyses suggest minimal shortening on the downslope direction (northeast). The resulting geologic map depicts structures and stratigraphic contacts in sufficient detail for paleohydraulic reconstruction.

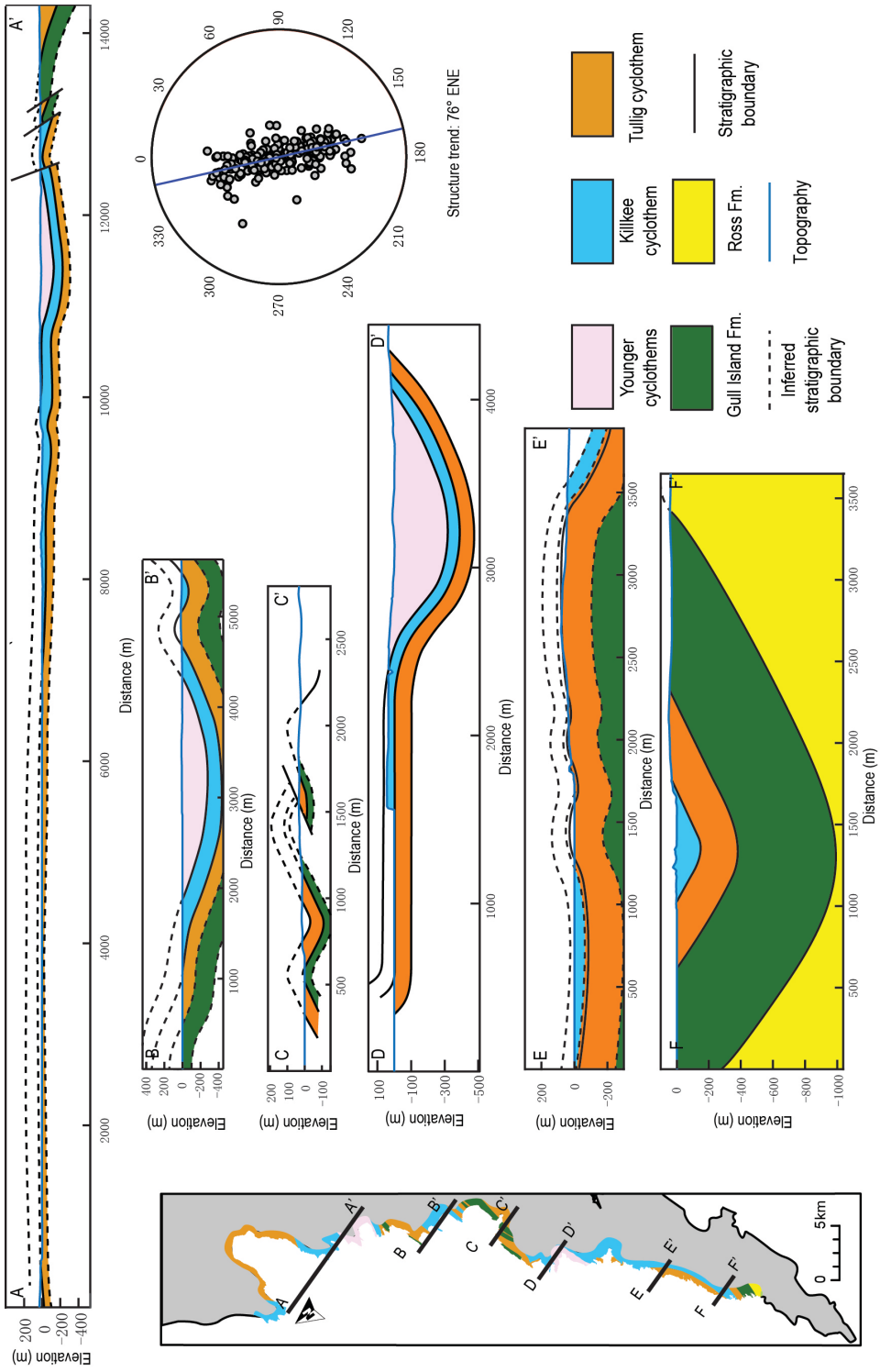

Figure S1: Geologic cross sections of characteristic first-order fault related folds deforming strata within the WINB. These structures typically have low amplitudes (~ 200 m) and kilometer scale wavelengths (500-1000 m). Sections AA' and BB' are shown in the same scale. The scales of sections

CC', DD, and FF' are individually adjusted to enhance readability. The locations of these lines of section are shown in the inset geological map. The lower hemisphere stereographic projection of poles to bedding measured in the WINB study area (n=203) suggest a regional structural trend of 076°ENE, which is roughly parallel to the paleocurrent direction.

Field Locations

The following table lists the geographic coordinates for the outcrop exposures of the Tullig Sandstone analyzed in this study. The 3D digital outcrop models (Wu, 2022) used for measuring bed thickness can be viewed at www.V3Geo.com (Table S1).

Table S1. Outcrop locations

Location	Coordinates		3D model
Tullig Point	52°36'40.08"N	9°48'11.64"W	https://v3geo.com/model/424
Trusklieve	52°37'48.40"N	9°46'51.81"W	https://v3geo.com/model/416
Castle Point	52°39'28.63"N	9°43'19.48"W	
Pulleen	52°44'35.46"N	9°36'25.03"W	https://v3geo.com/model/418
Killard (North)	52°45'4.44"N	9°33'14.35"W	https://v3geo.com/model/419
Killard (South)	52°45'5.84"N	9°32'56.24"W	https://v3geo.com/model/420
Carrowmore Point	52°46'9.66"N	9°30'9.79"W	https://v3geo.com/model/421
Furreera	52°56'12.30"N	9°25'52.28"W	https://v3geo.com/model/422

Uncertainty analysis

Since A is a scaling term, simulations with different values of A can produce very similar stratigraphy contingent on the model run times and rate of base level rise. For example, in the first set of simulation (Fig. 5B), there are multiple points with misfit value close to the best fit model at the slope value of 2.13×10^{-4}, suggesting similar associated stratigraphic geometry (i.e., length and thickness).

These points correspond to a different rate of base level rise and the same slope (Fig. 5B). Therefore, the associated value of A must be different for these points because there are only three parameters evaluated in the inversion analysis (S, R_{bl} and r_B) that can affect stratigraphic geometry. In this case, the values for the associated A are different because of different r_B (Eq. 3). This also suggests that estimates of both R_{bl} and r_B can be improved with additional constraints on other parameters (e.g., Λ, Ω, I_f). Therefore, the inversion analysis provides a relatively wide range of predictions for the rate of base level rise in the first set of simulations (Fig. 5C).

The uncertainty in modeled stratigraphy is mainly due to the natural variability in friction coefficient and bankfull depth of normal flow (Fig. S2A-B). Friction coefficient and flow depth set the spatial pattern in sediment flux (Eq. 2) and channel aggradation (Eq. 3), and thus in turn determine stratigraphy patterns. The value of the friction coefficient can span a wide range for a given channel slope (Fig. S2A and C), and may be very difficult to constrain. For lowland rivers ($S < 5\times10^{-4}$), a characteristic value of 0.005 is typically assumed for sand-bed rivers with median grain size around 250 – 500 μm (Chadwick et al., 2020) (Fig. S2C). However, for fine grained system where median grain size is less than 150 μm, such as the Tullig Sandstone, friction coefficient typically possesses a lower value (Moodie et al., 2019; Ma et al., 2022). Therefore, our choice for the low value of coefficient (0.0016, as Chezy friction coefficient in Parker et al., 2008b) is appropriate as it reflects the fine-grained nature of Tullig Sandstone.

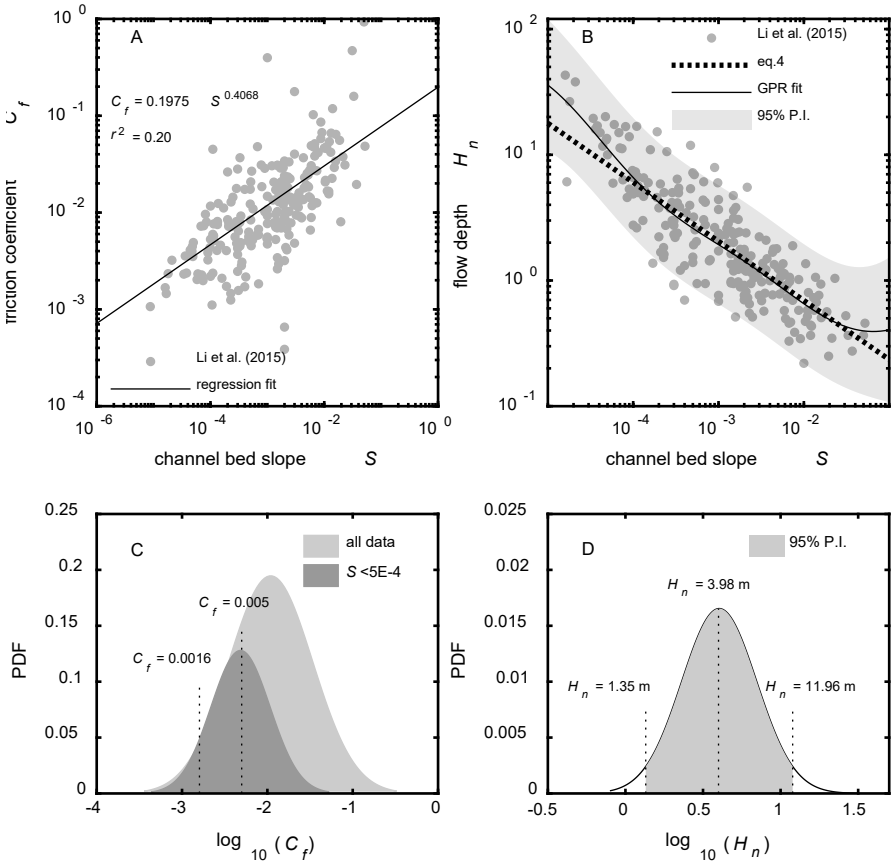

Figure S2. Channel bed slope *S* versus friction coefficient C_f of 231 rivers (Li et al., 2015) with a power regression fit (A). Channel bed slope *S* versus bankfull normal flow depth H_n of the same data set with a Gaussian Process Regression (GPR) fit and associated 95% prediction interval (P.I.) (B). Log-normally distributed friction coefficient for all 231 rivers and a subset of 79 lowland rivers ($S < 5\times10^{-4}$) (C). Probability density function of bankfull normal flow depth evaluated at channel bed slope of 2.13×10^{-4} based on Gaussian Process Regression (D).

To evaluate the uncertainty associated with the prediction of the flow depth, a Gaussian Process Regression (GPR) fit for the data from Li et al. (2015) is conducted and the result agrees with the theoretical relation (Eq. 4) especially for channel slopes ranging from $1 \times 10^{-4} – 1 \times 10^{-2}$ (Fig. S2B). While the prediction of bankfull normal flow depth from the GPR (4 m) for the best fit slope of $2.13 \times 10^{-}$

[4] agrees with the prediction using Eq. 4 (4.2 m), the 95% prediction interval (1.4 to 12 m) yielded by the GPR is much less constrained (Fig. S2D).

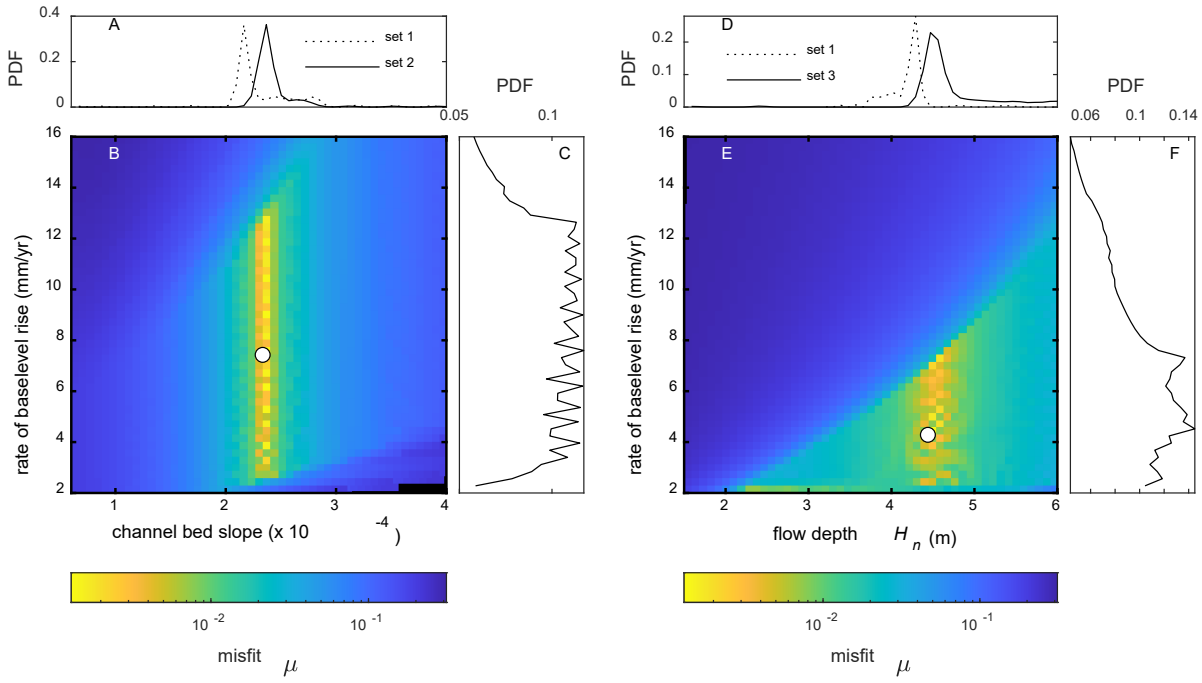

Figure S3. Inversion analyses for testing the sensitivity of model output to friction coefficient C_f (A-C) and bankfull normal flow depth H_n (D-F). Each cell in the heat maps represents the minimum misfit for a given set of R_{bl} and S (B) or R_{bl} and H_n (E) within the parameter space of r_B. Best fit model is marked by the white dot. Posterior probability density function (PDF) for R_{bl}, S and H_n are plotted along axes (solid lines) (A, C, D, F). PDF for S from the first set of simulation (dashed line) is also shown for comparison (A).

To test further the sensitivity of model output to C_f and H_n, we perform two more sets of simulations. The second set of simulation (Fig. S3A-C) differs from the first set of simulation (Fig. 5) in terms of the value of the friction coefficient (0.005) and the range of rate of base level rise (2 – 16 mm/yr). Similar to the first set of simulation, the second set of simulation also provides clustered predictions for slope (Fig. S3A) and dispersed prediction for rate of base level rise (Fig. S3C). The best fit model corresponds to a channel bed slope of 2.33×10^{-4} and a rate of base level rise of 7.4 mm/yr, which are very

close to the best fit predictions from the first set of simulation ($S = 2.13\times10^{-4}$ and $R_{bl} = 7.4$ mm/yr; Fig. 5 and Fig. S3). This result suggests that the sensitivity of model output to C_f of typical lowland rivers is limited: the slope prediction only shows a 9% increase with a C_f value that is a factor of three higher.

The third set of simulation evaluate input parameters of bankfull depth of normal flow H_n (1.5 – 6 m), rate of base level rise R_{bl} (2 – 16 mm/yr) and ratio between channel width and floodplain width r_B (10 – 50), while channel bed slope S is fixed at 2.13×10^{-4} (Fig. S3D-F). The best fit model corresponds to a bankfull normal flow depth of 4.4 m and a rate of base level rise of 4.3 mm/yr, with 95% credible intervals of 4.2 – 5.8 m and 2 – 15 mm/yr, respectively. The modeled stratigraphic geometry is very sensitive to H_n, as reflected by the wide range of model misfit (Fig. S3E). However, the uncertainty associated with the relation between channel bed slope and bankfull normal flow depth (Eq. 4, Fig. S2B and D) leads to limited uncertainty in predictions for flow depth. The predictions for bankfull normal flow depth H_n from the best fit models for the first and the third sets of simulations are very close (4.2 and 4.4 m, respectively). Moreover, even after incorporating a relatively dispersed prior distribution for flow depth calculated through GPR for channel bed slope S of 2.13×10^{-4} (Fig. S2D), the associated posterior distribution remains clustered (Fig. S3D).

References Cited

Chadwick, A.J., Lamb, M.P., and Ganti, V., 2020, Accelerated river avulsion frequency on lowland deltas due to sea-level rise: Proceedings of the National Academy of Sciences, v. 117, p. 17584–17590, doi:10.1073/pnas.1912351117.

Cooper, M.A., Collins, D.A., Ford, M., Murphy, F.X., Trayner, P.M., and O'sullivan, M., 1986, Structural evolution of the Irish Variscides: Journal of the Geological Society, v. 143, p. 53–61, doi:10.1144/gsjgs.143.1.0053.

Gill, W.D., 1962, The Variscan fold belt in Ireland, *in* Coe, K. ed., Some aspects of the Variscan fold belt, Manchester University Press, p. 44–64.

Lopez, A.R., Herbert, L.A., Wu, C., Sacklett, H.L., Giorgis, S.D., Burmeister, K.C., and Nittrouer, J., 2017, A companion of Rf/phi and AMS fabrics in strata involved in the Variscan fold-thrust belt; western Irish Namurian Basin, County Claire, Ireland, *in* Geological Society of America Abstracts with Programs, Seattle, Washington, USA, v. 49, p. 308721, doi:10.1130/abs/2017AM-308721.

Ma, H. et al., 2022, Amplification of downstream flood stage due to damming of fine-grained rivers: Nature Communications, v. 13, p. 3054, doi:10.1038/s41467-022-30730-9.

Moodie, A.J., Nittrouer, J.A., Ma, H., Carlson, B.N., Chadwick, A.J., Lamb, M.P., and Parker, G., 2019, Modeling Deltaic Lobe-Building Cycles and Channel Avulsions for the Yellow River Delta, China: Journal of Geophysical Research: Earth Surface, v. 124, p. 2438–2462, doi:10.1029/2019JF005220.

Murphy, J.B., Pisarevsky, S.A., Nance, R.D., and Keppie, J.D., 2001, Animated History of Avalonia in Neoproterozoic-Early Palaeozoic: Journal of Virtual Explorer, v. 3, p. 45–58.

Naylor, D., 1978, A structural section across the Variscan fold belt, southwest Ireland: Journal of Earth Sciences, p. 63–70.

Neuman, R.B., 1984, Geology and paleobiology of islands in the Ordovician Iapetus Ocean: Review and implications: Geological Society of America Bulletin, v. 95, p. 1188–1201.

Tanner, D.C., Bense, F.A., and Ertl, G., 2011, Kinematic retro-modelling of a cross-section through a thrust-and-fold belt: the Western Irish Namurian Basin: Geological Society, London, Special Publications, v. 349, p. 61–76.

Windley, B.F., 1995, The evolving continents: Chichester, England, Wiley, 526 p.

Wu, C., 2022, Three-dimensional Digital Outcrop Models of the Tullig Sandstone, Western Irish Namurian Basin, Co. Clare, Ireland:, doi:10.5281/zenodo.6781516, https://zenodo.org/record/6781516